

Effects of bioirrigation on the spatial and temporal dynamics of oxygen above the sediment–water interface

E. Murniati^{1,2,5}, D. Gross^{1,6}, H. Herlina^{1,7}, K. Hancke^{3,4,8}, and A. Lorke^{2,9}

¹Institute for Hydromechanics, Karlsruhe Institute of Technology, 76131 Karlsruhe, Germany

²Institute for Environmental Sciences, University of Koblenz-Landau, 76829 Landau in der Pfalz, Germany

³Department of Biology, Nordic Center for Earth Evolution, University of Southern Denmark, 5230 Odense M, Denmark

⁴Section for Marine Biology, Norwegian Institute for Water Research, 0349 Oslo, Norway

Abstract: Burrow ventilation by tube-dwelling benthic animals affects solute exchange between sediments and water by 2 means. Drawing of O₂-rich water into the burrow increases O₂ availability in the sediment and stimulates biogeochemical and microbial processes, whereas flushing of the burrow creates a 3-dimensional flow field above the burrow, which induces mixing. Previous studies have revealed the role of the diffusive boundary layer (DBL) thickness on the exchange of solutes between the sediment and overlying water. Mapping the O₂ gradient within the DBL is a challenging task in the presence of benthic faunal activities. We used a novel lifetime-based laser induced fluorescence (τ LIF) technique that enables unobstructed observations of spatial and temporal O₂ dynamics above burrows inhabited by midge larvae (*Chironomus plumosus*). We observed instantaneous plumes of O₂-depleted water released from the outlet of the burrows and drawdown of O₂-rich water above the inlet caused by peristaltic pumping of *C. plumosus* larvae. Vertical O₂ gradients changed dynamically during burrow ventilation relative to in a control tank without animals. The advective transport of O₂ above the opening caused by burrow ventilation degraded the O₂-concentration gradient. For a range of larvae densities that is frequently observed in ponds and lakes, the advective transport caused by burrow ventilation was the dominant transport mechanism.

Key words: oxygen flux, diffusive boundary layer, bioturbation, sediment–water interface, laser-induced fluorescence, oxygen-sensitive nanobeads

Bioturbation of aquatic sediments by benthic fauna was defined by Kristensen et al. (2012) as the combined effect of particle reworking (sediment movement) and burrow ventilation (water movement). Burrow ventilation by tube-dwelling benthic animals draws O₂-rich water through a burrow inlet and releases plumes of deoxygenated water through a burrow outlet. The ventilation creates complex 3-dimensional (3-D) concentration distribution in the sediment (Lewandowski and Hupfer 2005) and 3-D flow fields above the burrow (Morad et al. 2010, Roskosch et al. 2010). The enhanced O₂ flux into the sediment stimulates aerobic respiration and is accompanied by enhanced exchange of solutes between sediment and overlying water (Matisoff and Wang 1998, Mermillod-Blondin et al. 2004, Hölker et al. 2015). The enhancement of sediment O₂ uptake promoted by tube-dwelling benthic animals has been examined in numerous studies (Hargrave 1972, Pelegri and Blackburn 1996, Han-

sen et al. 1998, Matisoff and Wang 1998, Baranov et al. 2016b) and depends on the species present, their abundance, the overlying O₂ concentration, and temperature (Roskosch et al. 2012, Baranov et al. 2016a).

Tube-dwelling animals, such as *Chironomus plumosus* larvae, construct U-shaped burrows, some of which can extend up to 15 cm below the surface of the sediment (Granéli 1979b). For some benthic animals, such as *Pygospio elegans*, *Chironomus riparius*, and *Chironomus dorsalis*, the inlet of the tube typically extends a few millimeters above the surrounding sediment. This height is assumed to bypass the low-O₂-concentration region of the boundary layer overlying the sediment–water interface (SWI) (Jørgensen and Revsbech 1985, Pinder 1986, Stief et al. 2005).

The motion of *C. plumosus* that generates burrow ventilation takes the form of undulations of their ~20-mm-long body that travel in the head-to-tail direction as a sinu-

E-mail addresses: ⁵murniati@uni-landau.de; ⁶dieter.gross@kit.edu; ⁷herlina.herlina@kit.edu; ⁸kasper.hancke@niva.no; ⁹lorke@uni-landau.de

DOI: 10.1086/694854. Received 14 March 2017; Accepted 20 July 2017; Published online 28 September 2017.

Freshwater Science. 2017. 36(4):000–000. © 2017 by The Society for Freshwater Science.

000

soidal wave (Brackenbury 2000). This motion creates 3-D flow fields above the burrow inlet and outlet (Munksby et al. 2002, Morad et al. 2010, Roskosch et al. 2010). In alternating periods of pumping and resting, the larvae draw O₂-rich water into the burrow while pumping, absorb and store the O₂ in hemoglobin, and use the O₂ in the hemoglobin for metabolism during the periods of feeding or resting (Walshe 1950). *Chironomus plumosus* larvae adjust to low-O₂ conditions by becoming immobile and using the O₂ stored in the hemoglobin for up to 9 min (Walshe 1950).

The O₂ dynamics during bioturbation have been studied mainly in the sediments, and most observations from above the sediment surface are limited to flow velocities or pointwise concentration measurements. Flow-field observations based on particle image velocimetry (PIV) revealed the existence of large-scale plumes, particularly at the burrow outlets (Morad et al. 2010, Roskosch et al. 2010). The effect of these flows on the O₂-concentration distribution and mean vertical concentration gradients have not been investigated.

We used a recently developed lifetime-based laser induced fluorescence (τLIF) technique (Murniati et al. 2016) to analyze the effect of burrow ventilation of *C. plumosus* on the spatial and temporal O₂ dynamics above the SWI. The τLIF O₂ imaging system enables unobstructed observations of planar O₂-concentration dynamics above the SWI with high spatial resolution. We hypothesized that the diffusive boundary layer (DBL), which controls sediment–water fluxes of O₂ in the absence of bioirrigation (Lorke and Peeters 2006), becomes gradually degraded with increasing organism density. We analyzed the temporal dynamics of O₂-concentration distributions above burrows as a function

of organism density and in relation to their ventilation activity. We quantified the resulting mean O₂ gradients in the boundary layer and compared them to the nonbioturbated case to investigate the effect of bioturbation on the diffusive boundary-layer dynamics above the SWI.

METHODS

Experimental setup

We observed the dynamics of near-sediment O₂ distributions around natural burrows of *C. plumosus* in a series of laboratory experiments. We placed the organisms with varying abundance in 3 experimental chambers (tanks; 7 × 7 × 10 cm [length × width × height]), which were filled with 5 cm of sediment and 5 cm water (Fig. 1A). The sediment surface was slightly inclined (~12°) to permit an unobstructed view of the sediment surface, which was illuminated by the laser light sheet with a horizontally oriented camera (Fig. 1B). The experimental tanks (T1–T3) contained 3 (T1), 6 (T2), and 12 (T3) larvae corresponding to larval densities of 612, 1224, and 2448 individuals (ind)/m², respectively. An additional tank (T0) without larva provided a nonbioturbated control. During the experiment, all test tanks were closed with airtight transparent lids and kept in a water bath (40 × 30 × 22 cm) that maintained the temperature in the tanks at 21 ± 0.8°C. Except for the periods of laser illumination, we kept the tanks in the dark during the entire experiment.

Before placing the tanks in the water bath, we identified active burrows (Fig. 1C) in each tank by placing a fast-response O₂ sensor (FireStingO₂; Pyro Science GmbH, Aa-

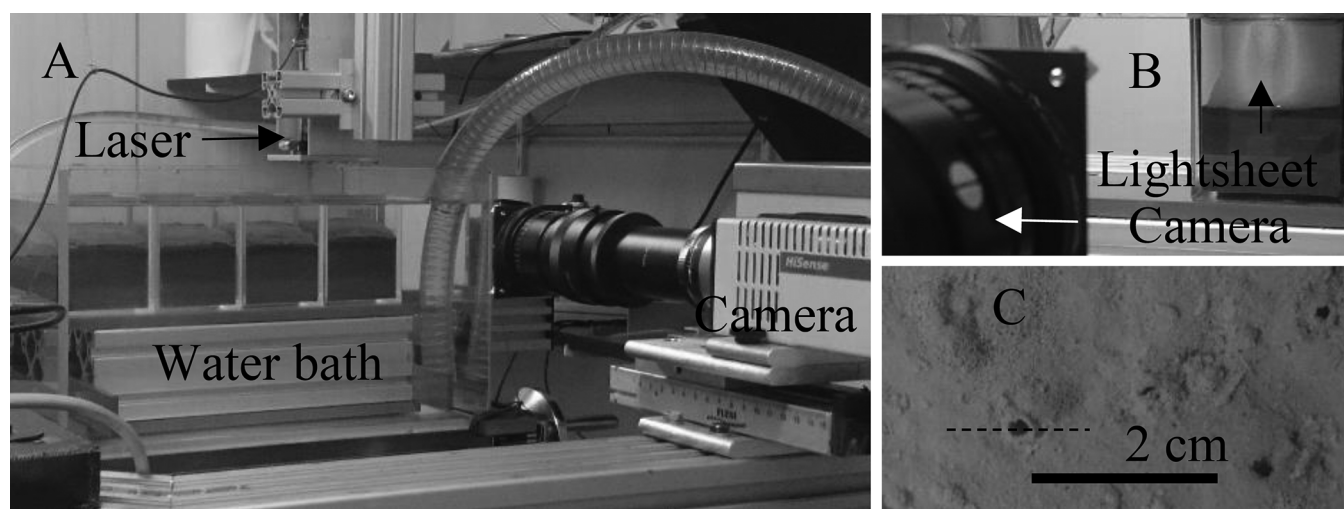


Figure 1. A.—Photograph of the experimental setup showing the 4 test tanks in the temperature-controlled water bath and the lifetime-based laser induced fluorescence (τLIF) system consisting of laser and camera. B.—Illustration of the projected laser light sheet from above and the illuminated area captured by the camera. The interrogation area was 14.4 × 19.2-mm. C.—Typical burrow openings in the test tank. The image was taken in T1 before the start of the experiment. The dashed line shows the location of the light sheet on the selected burrow opening.

Table 1. Experimental conditions in the 4 test tanks (T0–T3) including the starting and ending mean O₂ concentration during the measurement sequences, number and density (individuals/m² [in parentheses]) of chironomid larvae at the start and end of the experiments, and number (*n*) of measurement sequences (10 min of O₂ concentration imaging each). Numbers in parentheses are measurement sequences that passed the quality criteria and were used for analysis. * indicates that only the first 3 sequences were used for the mean vertical O₂-concentration profile analysis.

Test tank	Number and density of larvae			Bulk [O ₂] (μmol/L)
	Start	End	<i>n</i>	
T0	–	–	15 (10)	185–97
T1	3 (612)	2 (408)	15 (15)	191–154
T2	6 (1224)	6 (1224)	15 (15)	107–54
T3	12 (2448)	11 (2244)	15 (13*)	84–10

chen, Germany) close to the opening of each burrow. We observed the unobstructed spatial and temporal dynamics of O₂ concentrations around the selected burrow in- and outlets with the aid of planar (2-dimensional) lifetime-based laser-induced fluorescence (τLIF) measurements and suspended nanoparticles coated with an O₂ indicator (Murniati et al. 2016). The distances from the selected burrow opening to the nearest rigid walls were 1.5, 2.8, and 2.8 cm for T1, T2, and T3, respectively. The field of view used in T0 was at the center of the tank. We made hourly measurements of ~10-min duration each (300 concentration images) in all 4 tanks for a period of ~15 h (Table 1).

We added 0.35 mL of stock solution containing the O₂-indicator-coated nanobeads (equal to 0.24% of the volume of water in the tank) to each tank. The O₂ concentration in all tanks was adjusted sequentially to 80%-air saturation (220 μmol/L at 21°C) by purging with N₂ or re-aerating the water while mixing the O₂-indicator nanobeads in the tank. Thereafter, the tanks were closed. We report measurement times as relative time (hh : mm) after closing of the tanks.

Before the measurements, we conducted calibration experiments for converting fluorescence lifetime to O₂ concentration by varying the O₂ concentration in a tank (7 × 7 × 10 cm) with sediment but without animals. The same amount of O₂ indicator (0.24% of the volume of water) was used. The O₂ concentration was adjusted by purging the water with N₂ gas or atmospheric air. The calibration experiment was repeated after 30 h. During the final calibration, sodium sulfite (Na₂SO₃) was added in surplus to obtain an O₂ concentration of 0 μmol/L. In total, we observed 17 O₂ concentrations ranging between 0 and 272 μmol/L. For each of these O₂ concentrations, we collected 30 to 50 image pairs.

Sediment and organism preparation

We collected natural sediments from a small harbor at the Rhine River in Germersheim, Germany (lat 49.221717

N, long 8.382687 E), on 1 June 2016. We used an Ekman grab sampler to collect the upper 20 cm of sediment at a location ~3 m from shore at a depth of 3 m. We homogenized the sediment and passed it through a 1-mm sieve to remove debris and a 300-μm sieve to remove small organisms. We stored the sieved sediments in beakers at 4°C for 1 wk. Three days before introducing the larvae, we filled the test tanks with sediment and added tap water up to the rim.

We used cultured *C. plumosus* larvae (Amtrax Live Premium; Kölle Zoo, Karlsruhe, Germany) for the experiments. Cultured larvae have similar behavior to freshly collected organisms in bioirrigation experiments (Baranov et al. 2016b). We selected 4th-instar larvae based on body length (18–28 mm; Hilsenhoff 1966). We left the larvae in the test tank for 2 d to acclimatize and construct burrows. During this time, the water in the tanks was aerated continuously, and the tanks were covered by an insect net to prevent the escape of emerged adults. We counted the larvae remaining in the tanks at the end of the experiments.

τLIF setup We measured O₂ concentration by evaluating the fluorescence lifetime of Platinum(II)-5,10,15,20-tetrakis-(2,3,4,5,6-pentafluorophenyl)-porphyrin (PtTFPP) coated on nanobeads (diameter <500 nm) which were suspended in the water of all test tanks. We used the O₂-indicator nanobeads (PtTFPP) from the same batch as a previous study (Murniati et al. 2016). Fluorescence excitation was provided by short pulses from a 405-nm diode laser with a Powell lens, which expanded the laser beam into a 1-mm thick planar light sheet. We accumulated the fluorescence intensities within 2 distinct time windows (*W*₁ and *W*₂) following the excitation pulses for a number of individual excitations on separate images recorded by a 14-bit charge-coupled device camera (PCO.1600; PCO AG, Kelheim, Germany) with an electronic shutter. A sequencer unit generated the laser pulses and controlled the camera shutter. A detailed description of the fluorophores and the measurement system was given by Murniati et al. (2016).

We fixed the laser on a frame and illuminated the selected sediment surfaces from above. We placed the camera on a linear actuator plate to adjust the focus and mounted it on a vertically movable frame perpendicular to the light sheet. The setup enabled us to position the light sheet across a burrow opening and to adjust the focus of the camera to the position of the light sheet.

We optimized the operational parameters of the τ LIF measurements during preliminary tests to provide sufficient accuracy of individual O_2 -concentration measurements and a fast sampling rate (see Murniati et al. 2016 for a detailed description of these parameters and their effects on measurements performance). We used a duration of fluorescence excitation of 25 μ s, an equal exposure duration of 16 μ s in both time windows for fluorescence intensity measurements, and a delay of 10 μ s between both windows. We accumulated a train of 17,000 light pulses on each intensity image, resulting in a 2-s sampling interval for an integrated O_2 -concentration image. The spatial resolution of the concentration estimates was 12 μ m within a 14.4- \times 19.2-mm field of view.

τ LIF data processing We removed outliers in the recorded fluorescence intensity images by applying the phase-space method, an algorithm frequently applied for detecting spikes in acoustic Doppler velocimetry data (Goring and Nikora 2002). We replaced the outliers with values calculated from a cubic polynomial fitted to the remaining data. We smoothed the fluorescence lifetime distributions with a low-pass Gaussian filter with a 7- \times 7-pixel (84- \times 84- μ m) window size for noise reduction. We obtained final O_2 -concentration estimates by fitting the 2-site model (Sacksteder et al. 1993) to the lifetime estimates obtained from the calibration measurement. Fluorescence intensity decreased significantly during the experiments because of sedimentation or filtration of the fluorophore particles or photo-bleaching, but the pre- and post-calibration experiments provided consistent results (Fig. S1). Based on the performance estimates described by Murniati et al. (2016), we removed all measurement sequences for which the mean image intensity was <1100 , which is close to the level of camera noise (Fig. S2A–D). This process led to a reduction in available measurement sequences for subsequent analysis (Table 1).

SWI detection and vertical O_2 profiles

Bottom reflection of the laser light and high bead concentration resulting from sedimentation caused a pronounced fluorescence intensity maximum at the SWI. The vertical position of the SWI within the laser light sheet was detected as the local maximum in fluorescence intensity. We defined the SWI as 0 ordinate ($z = 0$) and moved all pixel columns accordingly. In some measurements, the SWI in the laser

sheet was partly blocked by sediment in front of the light sheet because of sediment reworking by the chironomids. The SWI region that was blocked by sediment was excluded from the mean O_2 -concentration profile calculation (Fig. S3A, B). In some cases, we could not observe the lower part (0.16–0.45 mm) of the vertical O_2 profile because of a combination of inclined sediment surface, thickness of the light sheet, and sedimentation of beads, so we extended the measurements to the SWI to define the O_2 concentration at the SWI (C_0) (cf. Fig. S3C). We defined the upper limit of the diffusive boundary layer (C_∞) as the intersection of the linear gradient of the O_2 concentration with the bulk-water O_2 concentration (cf. Fig. S4), calculated as the mean concentration in the extrapolated vertical profiles.

RESULTS

Sediment reworking

Chironomid larvae started burrow construction immediately after they were placed in the test tanks. One day after introducing larvae to the tanks, all organisms were in burrows. The sediment surface in all tanks was initially inclined and carefully trimmed to achieve a relatively smooth topography to ensure an unobstructed view on the illuminated plane (Fig. S3A). However, small-scale variation in the sediment topography is inevitable. Thus, locally elevated sediment surface between the illuminated plane and the camera occasionally blocked the camera's view of the actual sediment–water interface at the plane of interest. The treatment of such blocked area is explained in Fig. S3B.

In the tanks with chironomids, the sediment topography within the field of view changed throughout the measurement period (Fig. 2A–C). In T0, the sediment surface remained similar to its initial condition (<0.2 -mm vertical variations), but in the other tanks, vertical variation increased by as much as 4 mm. Temporal variation in the sediment surface was lower at the outlet (Fig. 2B) than around the inlet (Fig. 2A). These observations suggested that the modifications around the inlet were caused by direct sediment reworking of the chironomids, whereas around the outlet may have been caused by burrow ventilation and sedimentation of resuspended particles. In T3, a rapid change of the sediment topography around a burrow opening occurred between 10:01 and 11:20 h. Within 1 h, a chimney—a typical structure for an inlet—was formed (dotted line in Fig. 2C), and we observed a change of the O_2 -concentration structure above the opening from predominantly release of deoxygenated plumes to predominantly drawdown of O_2 -rich water (see further explanation in O_2 dynamics below). The altered O_2 structure above the opening might have been caused by undulation of the larva in the burrow in reverse direction or by a change in the orientation of the larva within the burrow.

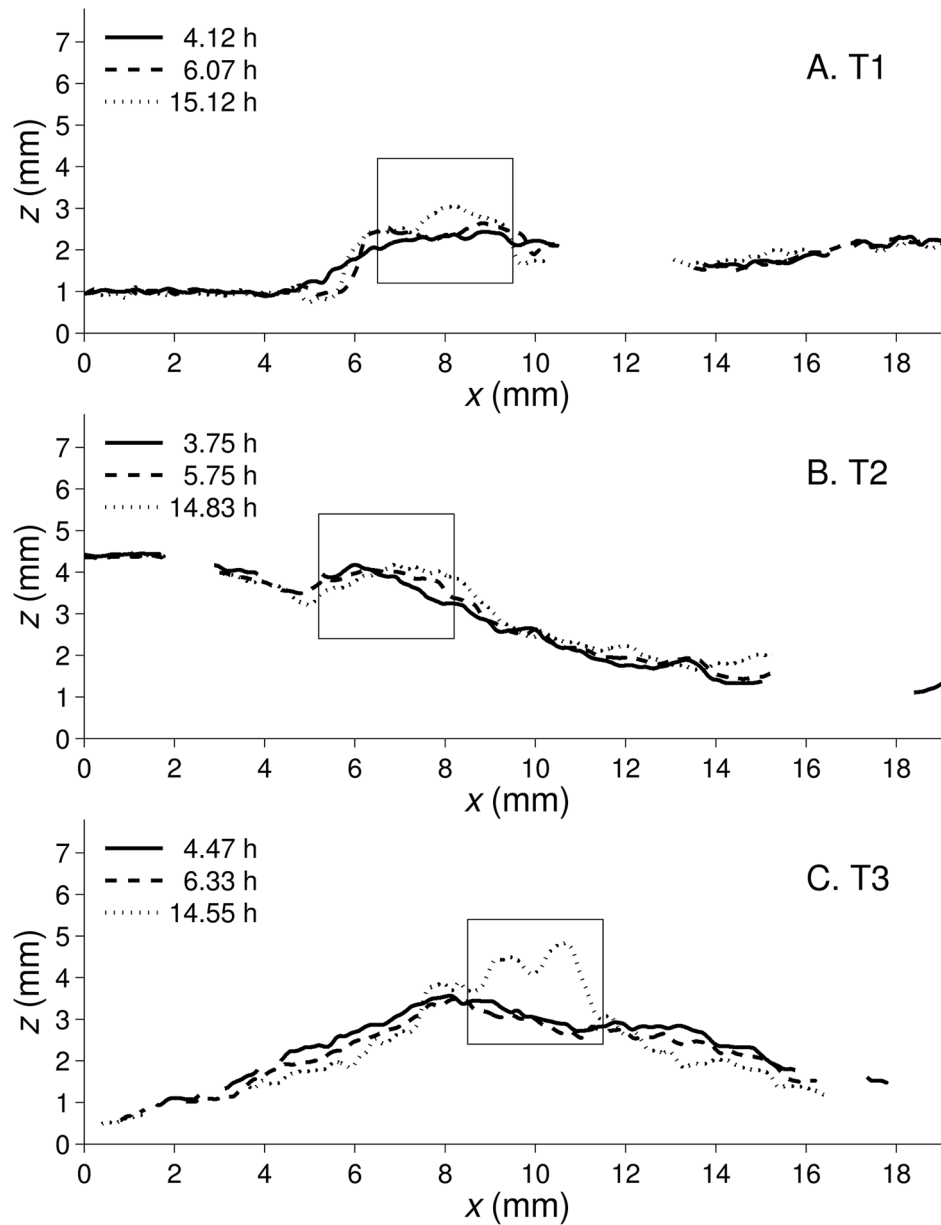


Figure 2. The sediment–water interface (SWI) in the camera field of view showing the burrow inlet in T1 (A), burrow outlet in T2 (B), and burrow opening in T3 (C) at selected measurement times indicated in the legend. The vertical coordinate (z) corresponds to the distance from the SWI. The location of the burrow opening is indicated by the bounding box. Breaks in the lines are the regions where the camera view of the SWI was blocked by elevated sediment between the light sheet and the camera.

O₂-concentration dynamics above burrows

Burrow ventilation was associated with the release of upward-propagating pulses of water with low O₂ concentration (Fig. 3A–C). The concentration in the initial plume of a pulse sequence could be as low as 10% saturation, but increased over time in subsequent pulses, indicating flushing of the burrow with water having higher O₂ concentration. The individual plumes propagated upward and developed into a mushroom-like shape while spreading horizontally

and entraining ambient water (Fig. 3C). The horizontal extent of the plumes was typically ~ 4 mm, whereas the vertical dimension often exceeded the field of view (>8 mm).

Particularly during periods of sustained pumping activity (e.g., at low O₂ concentration in T3), the upward propagating plumes drove coherent vortices, with outward flow at the top of the plume and inward-directed flow at the bottom. With these vortices, which had dimensions exceeding the size of the field of view, water from heights >1 cm above

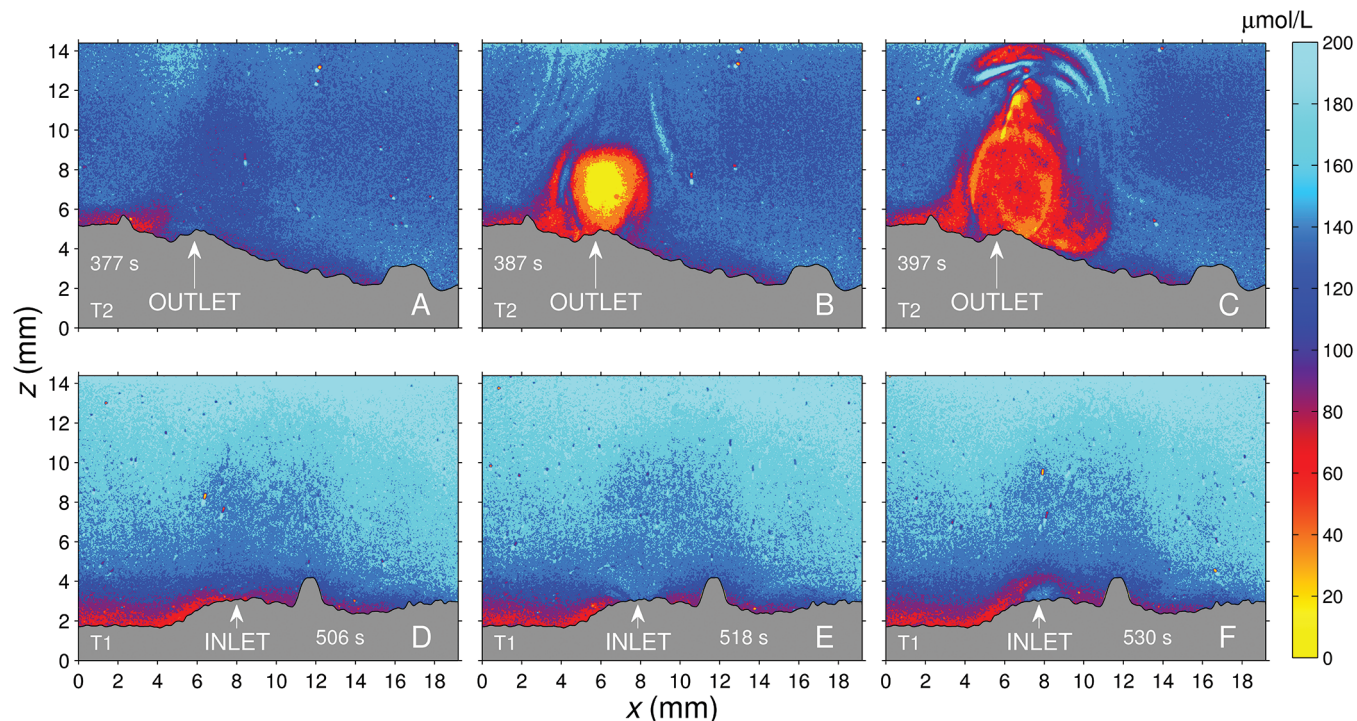


Figure 3. Sequences of O_2 -concentration distribution above a burrow outlet in T2 with a 10-s time interval between selected images (A–C) and a burrow inlet in T1 with a 12-s time interval between selected images (D–F). Animated sequences of both concentration distributions are available as supplementary videos V1 and V2.

the SWI with high O_2 concentration was continuously transported toward the sediment surface.

Visual analysis of subsequently observed concentration distributions indicated that plume velocities were mostly in the range of 0.6 to 2.1 mm/s with a maximum value of 4.8 mm/s (T2, +15 h). In T2 and T3, we occasionally observed packages of water moving into the field of view from the side. These packages probably were advected by larger-scale flow structures from neighboring burrow outlets.

Above the burrow inlet in T1 (Fig. 3D–F), the O_2 -concentration distribution was less dynamic. During pumping events, the bulk O_2 was drawn into the burrow where the maximum drawdown occurred in the center of the opening and extended up to 2 mm above the SWI (Fig. 3E). Within a radius of 1 to 3 mm around the burrow inlet, the O_2 concentration was highly affected by the drawdown, whereas at larger distances from the opening the concentration was less dynamic and more homogeneous. At the end of a pumping period (a sequence of pulses) or during periods of rest, we occasionally observed the release of small amounts of low- O_2 water from the inlet (Fig. 3F). We attribute this rather unexpected observation to small currents produced by movements of chironomids in the burrow during feeding or net construction. This interesting behavior was also found above the burrow opening in T3, where the observed O_2 structure was variable. In some sequences, the O_2 drawdown into the burrow was more dominant than the release

of deoxygenated plumes. The peculiar O_2 structures observed in T3 might be related to sediment reworking by the larva during chimney construction, as indicated by a significant increase of the sediment surface around the burrow opening (cf. Fig. 2C). The O_2 -concentration distribution in the tank without chironomids (T0) was horizontally more homogeneous and did not show significant short-term dynamics. In contrast to the observations above chironomid burrows, the O_2 gradients were restricted to a thin layer above the SWI.

Temporal dynamics of ventilation activity

Burrow ventilation was characterized by pulses of flow above openings and resulted in distinct O_2 structures above the burrow inlet (cf. Fig. 3D, E, Video V1) and outlet (cf. Fig. 3A–C, Video V2). Based on visual inspection of the concentration video sequences, we categorized observations into ventilation and resting periods. We observed pulses of flow during individual ventilation events and defined duration of active ventilation in a measurement sequence as the sum of the duration of individual ventilation events (summarized in Table 2). During an individual ventilation event, pumping pulses were created approximately every 8 s. In T1 and T2, an average of 3 ventilation/pumping events with durations of ~2.5 min were observed during the 10-min measurement sequences, and the larvae spent ~50% of the time

Table 2. Mean (\pm SD) values summarizing ventilation activity in the test tanks. Numbers in parentheses show larval density (individuals/m²). Four hours after the first measurement, the O₂ concentration in T3 was <15 μ mol/L. Eleven hours after the first measurement, the pumping activity in T3 was no longer detected in the concentration image.

Test tank	Pumping activity (min)		% time spent pumping	Individual pumping events	
	Pumping	Resting		Duration (min)	Number
T1 (612)	5.1 \pm 2.0	5.5 \pm 2.1	48 \pm 19	2.3 \pm 1.5	3 \pm 1
T2 (1224)	6.5 \pm 1.7	4.1 \pm 1.7	62 \pm 14	2.6 \pm 1.4	3 \pm 2
T3 (2448)	8.3 \pm 1.8	2.4 \pm 2.2	78 \pm 19	5.3 \pm 3.3	2 \pm 1

engaged in active burrow ventilation. In both tanks, ventilation activity varied strongly among the measurement sequences. The ventilation activity in T3 was comparable to that in the other 2 tanks for the first 4 h of measurements only, before the duration of the ventilation sequences increased strongly. On average, the duration of the ventilation sequences in T3 was 2 \times high as in T1 and T2, and the larvae spent nearly 80% of their time on burrow ventilation (Table 2). Uninterrupted ventilation activity was observed during some measurement sequences. The observed differences in pumping activity in T3 probably were related to the low O₂ concentration in this tank. The combination of data from the 3 tanks revealed a decreasing trend of pumping activity with increasing bulk O₂ concentration (Fig. 4). The observed fraction of venting decreased from nearly 100% at O₂ < 10% saturation to ~50% at O₂ saturation ~60%.

Mean vertical O₂ gradients

Mean vertical gradients of dissolved O₂ above the SWI were estimated by lateral averaging of the entire field of view (412–1045 pixel columns) and temporal averaging of all con-

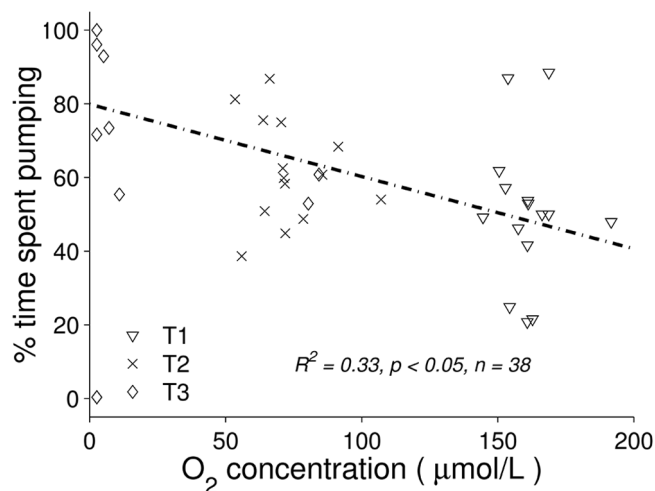


Figure 4. Percentage of time spent pumping vs O₂ concentration in the 3 test tanks. The dashed/dotted line shows a linear regression. O₂ saturation corresponded to a concentration of 280 μ mol/L.

centration images in a measurements sequence (249–436 concentration images). The resulting profiles differed substantially among the 4 tanks and measurement times (Fig. 5A–D).

In the control tank, the profiles were characterized by 2 nearly linear sections, with the stronger vertical gradient within the lowest 1 to 3 mm above the SWI (Fig. 5A). Above this concentration boundary layer, we observed a weaker, but persistent vertical gradient that can be attributed to the slow rates of vertical mixing in the stagnant tanks. Both bulk concentration and the O₂ concentration at the SWI decreased over time.

The profiles in T1 (low chironomid density) had a shape similar to those observed in the control tank, but the temporal decrease of O₂ concentration was much less pronounced (Fig. 5B). We attribute this to a potential leakage at the lid of T1 (see below). The mean vertical concentration gradients in T2 and T3 were much weaker (Fig. 5C, D), and in contrast to the control tank (T0), the gradient in the lower part of the profiles gradually decreased over time. In T3, the concentration dropped below 15 μ mol/L after the first 4 h of the experiment and was characterized by a constant weak O₂ gradient over the observed depth range.

DBL layer fluxes

In the absence of bioirrigation, sediment O₂ uptake rate is controlled by sediment O₂ demand and the diffusive O₂ flux across the waterside concentration boundary layer. At steady-state the sediment O₂ uptake rate can be described as the product of a transfer velocity and the concentration gradient (Lorke and Peeters 2006):

$$F_{DBL} = \frac{D}{\delta_{DBL}} (C_{\infty} - C_0) \quad \text{Eq. 1}$$

where F_{DBL} is the O₂ flux, D is the diffusion coefficient of O₂ ($D = 2.4 \times 10^{-5}$ cm²/s at 21°C), C_{∞} is the concentration at the upper end of the DBL, δ_{DBL} is the thickness of the DBL, and C_0 is the O₂ concentration at the SWI. The conceptual basis of Eq. 1 limits its application to T0, where the transport can be considered to be governed by diffusion only. In T0, the observed δ_{DBL} increased continuously over time to >3 mm at the end of the experiment (Fig. 6A). The 3-fold increase of δ_{DBL} led to a corresponding decrease of the O₂ flux across

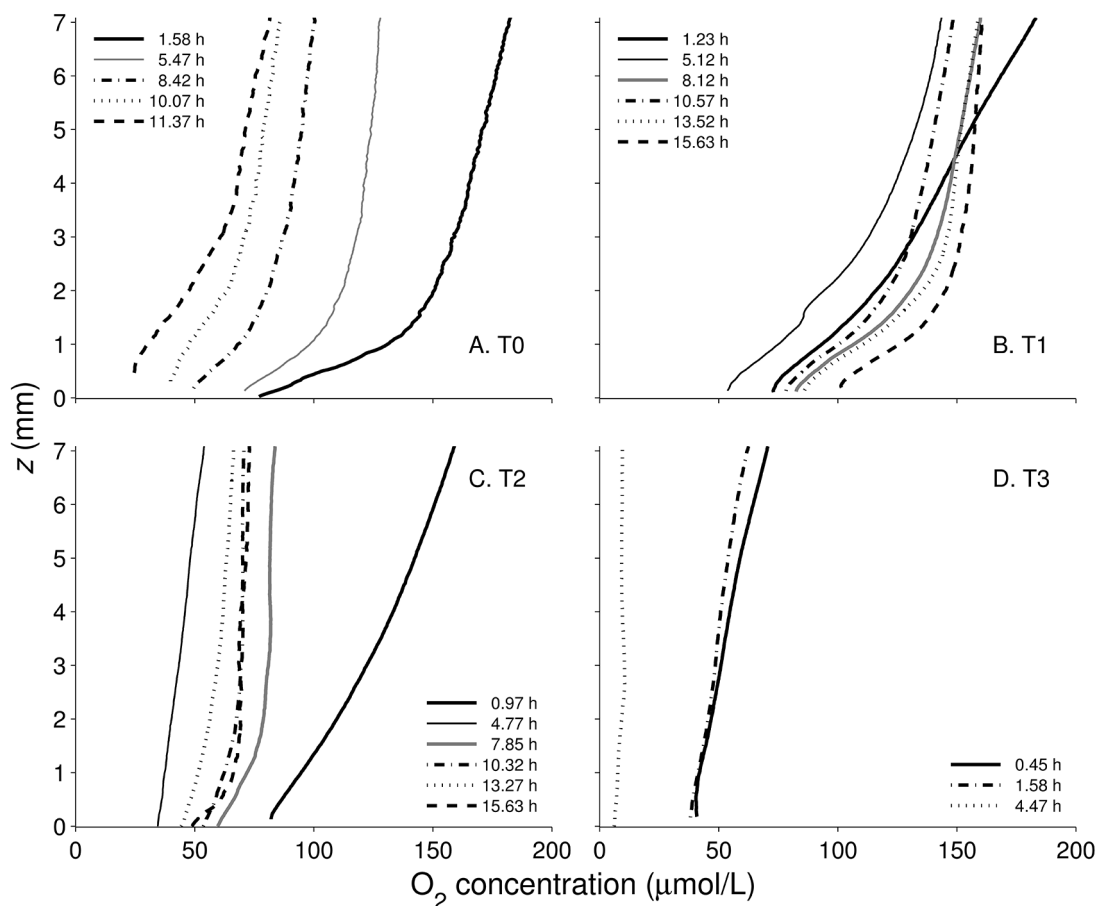


Figure 5. Mean vertical O_2 -concentration profiles in T0 (A), T1 (B), T2 (C), and T3 (D) at selected measurement times indicated in the legend. The vertical coordinate (z) corresponds to the distance from the sediment–water interface, and the profiles were averaged laterally over the entire field of view and temporally over the entire measurement sequence (10 min).

the SWI from 12 to 3 $\text{mmol m}^{-2} \text{d}^{-1}$. Despite the broad range of temporal variability of δ_{DBL} (Fig. 6A) and O_2 concentration (Fig. 5A), the presentation of mean vertical O_2 profiles in a dimensionless form based on z/δ_{DBL} vs $(C - C_0)/(C_\infty - C_0)$ collapsed into a universal shape within the diffusive boundary layer (Fig. 6B). Above the DBL, the O_2 -concentration gradient also varied with time in the dimensionless presentation. These variations probably can be attributed to the variability of the weak, large-scale convectively driven mixing in the tank.

O_2 consumption and tentative mass balance

We estimated the mean O_2 concentration in the water column above the SWI by extrapolating the upper part of the laterally averaged concentration profiles (Fig. 5A–D) to the water surface and subsequent vertical averaging over the entire water column. Within the first 6 h of observations, the mean O_2 concentrations in T0 and T1 decreased at a similar rate, whereas they decreased much faster in T2 and T3 (Fig. 7). The concentration in T3 dropped to $<15 \mu\text{mol/L}$ during this time, but it approached rather constant values of

~ 70 and $150 \mu\text{mol/L}$ in T2 and T1, respectively. We assume that the unexpected stagnation of the mean O_2 concentration in T1 and T2 was caused by leakage and atmospheric aeration at the lids of these tanks. Therefore, we restrict the following analysis of the O_2 mass balance to the first 6 h of measurements, where a consistent decrease of O_2 concentration could be observed in all tanks.

For T0, we compared the observed rate of decrease of mean O_2 concentration with the rate resulting from the O_2 flux across the SWI (Eq. 1):

$$C_{DBL}(t_i) = C(t_{i-1}) - \frac{A}{V} F_{DBL}(t_i)(t_i - t_{i-1}), \quad \text{Eq. 2}$$

where $C(t_{i-1})$ and C_{DBL} are the initial concentration and the predicted concentration at some later sampling time (t_i), respectively. A (50 cm^2) and V (160 mL) are sediment surface area and volume of water, and F_{DBL} is the flux across the SWI estimated from DBL thickness (Eq. 1, Fig. 6A). The observed decrease of O_2 concentration in the water column of T0 was in very good agreement with the concentration estimated from Eq. 2 (Fig. 7), indicating that the DBL fluxes esti-

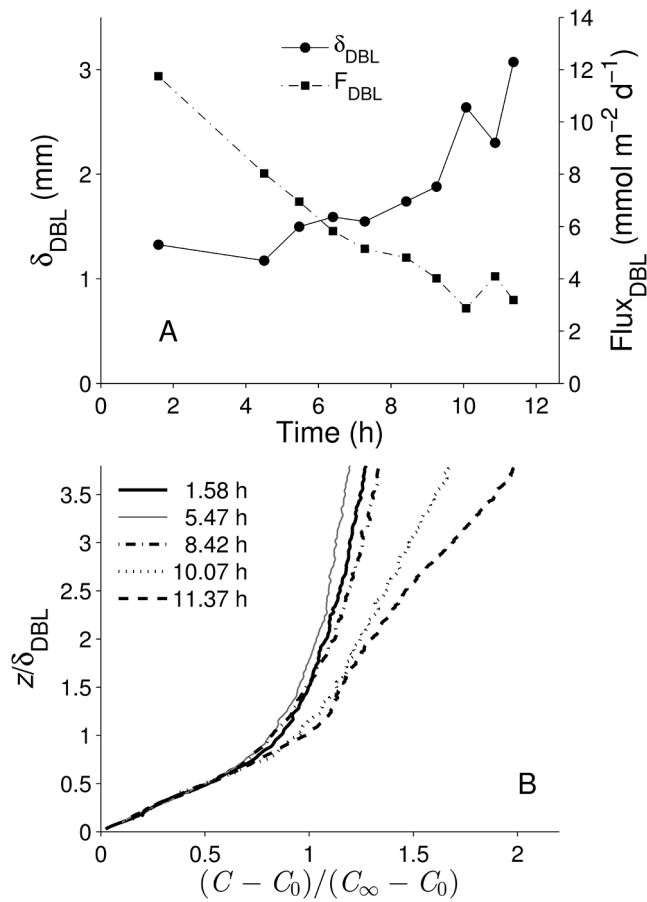


Figure 6. A.—Time series of the height of the diffusive boundary layer (δ_{DBL}) and the corresponding O_2 flux across the sediment–water interface (SWI) in T0. B.—Normalized (nondimensional) mean O_2 profiles in T0 for selected measurement times (cf. Fig. 5A). The vertical coordinate (z) was normalized using δ_{DBL} , whereas the O_2 concentration (C) was normalized using the difference between the bulk concentration (C_∞) and the concentration at the SWI (C_0).

mated from the vertical concentration gradient were representative for the entire tank and that no other sources or sinks for O_2 were present in T0.

To compare the O_2 dynamics in the tanks with chironomid larvae to that in T0, we estimated the sediment–water O_2 flux, which corresponds to the observed concentration decrease in the water during the first 6 h of observation ($F_{dC/dt}$; Table 3). The flux was comparable in T0 and T1, but it was increased by factors of 2.2 and 2.5 in T2 and T3, respectively. We estimated the contribution of organism respiration to the observed areal O_2 flux in the tanks by multiplying literature-based respiration rates of *C. plumosus* by larval density in the test tanks (Table 3). Depending on the particular choice of chironomid respiration rate, the observed flux enhancement by burrow ventilation exceeded the respiratory O_2 demand of the chironomids by up to a factor of 3.8 (Table 3).

DISCUSSION

Our study yielded the first unobstructed observation of the spatial and temporal dynamics of O_2 concentration above a sediment–water interface in the presence of infaunal activity. Planar O_2 -concentration dynamics above the sediment–water interface created by burrow ventilation by midge larvae (*C. plumosus*) were revealed and enabled visualization of small-scale fluid mechanics generated by activity of benthic organisms. Application of this novel τ LIF O_2 imaging system demonstrated its ability to resolve benthic DBL dynamics. Thus, it facilitates a more detailed analysis than has been possible in the past of O_2 -transport mechanisms across the sediment–water interface under complex conditions.

The fluorescence intensity signal decayed during the measurements (Fig. S2), indicating a decrease of nanobead concentration or photo-bleaching of the O_2 indicator coating. The filtration efficiency of *C. plumosus* has been reported to be highest for particles $>17\ \mu m$ in diameter (Walshe 1947). Therefore, we expected that the small ($<0.5\ \mu m$) O_2 -sensing nanobeads would be affected by filtration to a lesser extent. However, the nanobeads were subject to agglomeration and the observed intensity reduction was most probably related to settling, as indicated by the observed increase of fluorescence intensity at the sediment surface (Fig. S3), and to filter-feeding by the larvae, as indicated by the relatively higher reduction of intensity in tanks with higher larval density (Fig. S2). We did not test photo-bleaching of the O_2 -indicator nanobeads (PtTFPP), but PtTFPP has a photostability similar to that of ruthenium and is less susceptible to photo-bleaching than platinum octaethylporphyrin (PtOEP) (Yeh et al. 2006, Borisov and Klimant 2009, Papkovsky and Dmitriev 2013). Nevertheless, the lifetime-based measurement principle makes the τ LIF O_2 imaging system indepen-

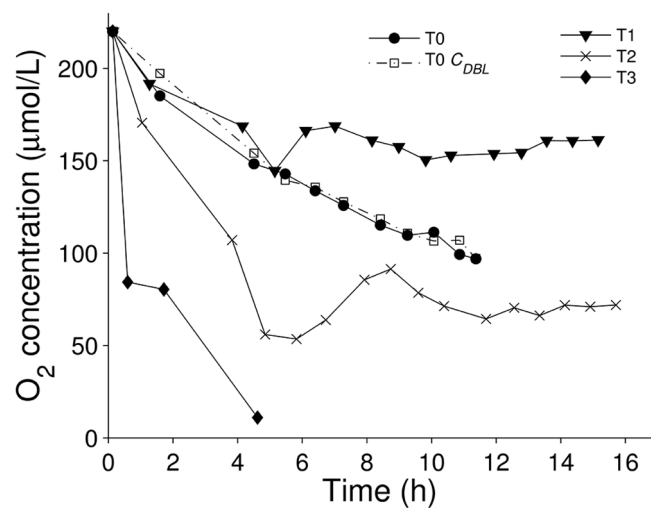


Figure 7. Time series of mean O_2 concentration (C) in the 4 experimental tanks and the decrease of the initial O_2 concentration in T0 calculated from the estimated diffusive boundary layer (DBL) fluxes (Eq. 2).

Table 3. Components of the O₂ mass balance in the 4 experimental tanks during the first 6 h of the experiment. O₂ flux across the sediment–water interface (SWI) is the observed rate of change of O₂ concentration in the water ($F_{dC/dt} = \frac{V}{A} \frac{dC}{dt}$), where F_{resp} = areal O₂ flux corresponding to chironomid respiration (larval density × individual respiration rate), the range corresponds to respiration rates between 2.9 μmol d⁻¹ larva⁻¹ (Granéli 1979b) and 6.5 μmol d⁻¹ larva⁻¹ (Soster et al. 2015), $\frac{F_{dC/dt}}{F_0}$ is flux enhancement factor relative to diffusive O₂ flux in T0 (F_0), and $\frac{F_{dC/dt} - F_0}{F_{resp}}$ is the ratio of the enhanced flux to chironomid respiration (the range of flux corresponds to the range of F_{resp}). The number in parentheses shows larval density (individuals/m²).

Test tank	$F_{dC/dt}$ (mmol m ⁻² d ⁻¹)	F_{resp} (mmol m ⁻² d ⁻¹)	$\frac{F_{dC/dt}}{F_0}$	$\frac{F_{dC/dt} - F_0}{F_{resp}}$
T0 (0)	10.8	0	1	–
T1 (612)	10.1	1.8–4.0	0.94	–0.4 to –0.2
T2 (1224)	24.2	3.5–8.0	2.2	3.8–1.7
T3 (2448)	27.0	7.1–16	2.5	2.3–1.0

dent of O₂-indicator nanobead concentration and light distribution (Murniati et al. 2016) and independent of the reduction in the intensity signal (Fig. S1).

The abundance of organisms used in our experiments (corresponding to 0–2448 larvae/m²) covered the range of *C. plumosus* densities frequently observed in ponds and lakes around the globe (Granéli 1979b, Hölker et al. 2015, Soster et al. 2015). Moreover, larval behavior during the experiments and their activity patterns agreed with observations from previous laboratory studies. Fine-scale O₂ measurements showed pumping activity in all bioturbated tanks during the 1st measurement sequence, indicating that experimental handling procedures did not greatly inhibit chironomid activity. By comparing different measurement techniques, an average percentage of pumping activity of ~50% of the total observation period also was estimated by Roskosch et al. (2011), with individual pumping sequences lasting, on average, 2.75 min at 20–23°C and 100% O₂ saturation. Similar to our observations, pumping activity increased from ~50% at O₂ saturation to nearly 100% under hypoxic (<20% saturation) conditions (Walshe 1950). Besides burrow ventilation, the chironomids actively changed the small-scale sediment topography by constructing chimneys at the burrow inlets. Our observations clearly demonstrate that the up to 2-mm tall elongations of the burrow inlets potentially tower over the DBL above the surrounding sediment surface and, thereby, bypass the low-O₂-concentration zone. Chimney construction has previously been described for *Chironomus riparius* larvae when exposed to hypoxic conditions (Stief et al. 2005).

Previous observations of burrow ventilation were focused mainly on the spatial and temporal dynamics of O₂ and other solutes within the sediment (Lewandowski and Hupfer 2005, Polerecky et al. 2006, Glud 2008, Baranov et al. 2016a, b). Observations on the water side of the SWI have been restricted to pointwise concentration measurements with microelectrodes (Roskosch et al. 2011, Soster et al. 2015) or to observations of the flow fields associated with burrow ventilation using PIV measurements (Morad et al. 2010, Roskosch

et al. 2010). Anoxic or suboxic plumes in the overlying water were documented in the presence of a wide range of marine benthic organisms with the aid of planar optodes (Volkenborn et al. 2010, Woodin et al. 2010). However, these observations were limited to information next to rigid walls, which potentially affected plume dimensions and dynamics. The high-spatial resolution of the τ LIF system applied in our study allowed us to quantify the dynamics of O₂-concentration gradients in the top few millimeters above the sediment surface. The observed spatial dimensions of the drawdown zones above burrow inlets and of the released plumes above the outlets principally agreed with measurements of the respective flow fields (Morad et al. 2010, Roskosch et al. 2010), but our measurements revealed the persistence of pumping-induced changes in the O₂ dynamics above the sediment–water interface. In the absence of bioturbation, O₂ transport into the sediment is limited by a DBL. The thickness of the DBL and, therefore, the O₂ flux, is modulated by bottom boundary-layer turbulence driven by large-scale flows in the respective aquatic system (Lorke et al. 2003, 2012, Murniati et al. 2015). The DBL thickness and corresponding sediment–water fluxes of O₂ observed in the control tank without chironomids (T0) were in the range of those values observed in a lake during periods of weak hydrodynamic forcing (Bryant et al. 2010). However, this relationship was altered completely by advective O₂ transport and the larger-scale mixing that was particularly generated by the energetic plumes released at the burrow outlet in the presence of chironomids. Our results demonstrated that even for the lowest organism density, O₂ transport became dominated by bioturbation that caused a complete change of the concentration boundary layer. Our experiments were conducted without significant background flow, but this finding suggests a regime shift from physical (large-scale flow fields driving bottom-boundary-layer turbulence) in the absence of bioturbation to biological (abundance and species composition of bioturbating fauna in the sediment) control of sediment O₂ uptake in the presence of bioturbating fauna. The biological control can result in strongly

enhanced fluxes, but it is likely to have a different temperature-dependence (Roskosch et al. 2012, Baranov et al. 2016a) than that of the hydrodynamic control or microbial O₂ consumption rate in the sediments (Murniati et al. 2015) and, therefore, can be expected to have different seasonal dynamics.

The effect of burrow irrigation on the O₂ dynamics above the sediment–water interface can be expected to depend on burrow depth and length, which we did not measure. The chosen sediment thickness of 5 cm may have been a limiting factor in our experiments. A wide range of the tube depths below the sediment surface has been observed. Granéli (1979b) reported that the tubes can penetrate up to 15 cm into the sediment. Walshe (1950) found that the tubes usually extended to a depth of 3 to 6 cm, similar to what was reported by Soster et al. (2015). Nevertheless, in accordance with previous observations for similar larval density of 2000 ind/m² (Polerecky et al. 2006, Soster et al. 2015, Baranov et al. 2016b), the areal O₂ uptake rates of the sediment increased up to 2.5× in the presence of chironomids in comparison to the diffusive flux in the control tank. Assuming a respiratory O₂ demand by the organisms at the lower end of published data, the enhanced O₂ flux into the sediment exceeded the demand by up to a factor of 4, which confirmed the potential importance of the prevailing controlling mechanism (physical vs biological) for mineralization rates and therewith for nutrient and C cycling in aquatic ecosystems (Granéli 1979a, Hölker et al. 2015, Glud et al. 2016).

Given the potential significance of biological vs physical control of sediment–water fluxes, future investigators should aim at a more realistic representation of both processes and address mutual interactions of benthic boundary layer flow and bioirrigation. Such measurements ideally would combine flow-field observations based on particle image velocimetry (Morad et al. 2010, Roskosch et al. 2010) with τ LIF concentration imaging under defined background flow conditions in the laboratory or in-situ without obstruction of the natural flow field.

ACKNOWLEDGEMENTS

Author contributions: EM contributed to the experimental design, conducted the experiments, analyzed the data, and prepared the initial manuscript. DG provided his expertise in technical setup of the τ LIF system. HH contributed to the detailed experimental design and together with EM analyzed the data under supervision of AL. AL proposed the idea and developed the concept of the experiment. KH prepared the O₂-indicator-coated nanobeads and provided expertise related to the experimental design and data assessment presented in the manuscript. All authors reviewed the manuscript and gave final approval for publication.

We thank the German Research Foundation (DFG, UH 242/6-1) for funding EM, HH, and DG. EM was also supported by a scholarship from the University of Koblenz-Landau. Constructive comments from Nils Volkenborn and 1 anonymous referee greatly helped to improve the clarity of the final manuscript.

LITERATURE CITED

- Baranov, V., J. Lewandowski, and S. Krause. 2016a. Bioturbation enhances the aerobic respiration of lake sediments in warming lakes. *Biology Letters* 12:20160448.
- Baranov, V., J. Lewandowski, P. Romeijn, G. Singer, and S. Krause. 2016b. Effects of bioirrigation of non-biting midges (Diptera: Chironomidae) on lake sediment respiration. *Scientific Report* 6:27329.
- Borisov, S. M., and I. Klimant. 2009. Luminescent nanobeads for optical sensing and imaging of dissolved oxygen. *Microchimica Acta* 164:7–15.
- Brackenbury, J. 2000. Locomotory modes in the larva and pupa of *Chironomus plumosus* (Diptera, Chironomidae). *Journal of Insect Physiology* 46:1517–1527.
- Bryant, L. D., C. Lorrai, D. F. McGinnis, A. Brand, A. Wüest, and J. C. Little. 2010. Variable sediment oxygen uptake in response to dynamic forcing. *Limnology and Oceanography* 55:950–964.
- Glud, R. N. 2008. Oxygen dynamics of marine sediments. *Marine Biology Research* 4:243–289.
- Glud, R. N., P. Berg, H. Stahl, A. Hume, M. Larsen, B. D. Eyre, and P. L. M. Cook. 2016. Benthic carbon mineralization and nutrient turnover in a Scottish sea loch: an integrative in situ study. *Aquatic Geochemistry* 22:443–467.
- Goring, D., and V. Nikora. 2002. Despiking acoustic Doppler velocimeter data. *Journal of Hydraulic Engineering* 128:117–126.
- Granéli, W. 1979a. The influence of *Chironomus plumosus* larvae on the exchange of dissolved substances between sediment and water. *Hydrobiologia* 66:149–159.
- Granéli, W. 1979b. The influence of *Chironomus plumosus* larvae on the oxygen uptake of sediment. *Archiv für Hydrobiologie* 87:385–403.
- Hansen, K., S. Mouridsen, and E. Kristensen. 1998. The impact of *Chironomus plumosus* larvae on organic matter decay and nutrient (N, P) exchange in a shallow eutrophic lake sediment following a phytoplankton sedimentation. *Hydrobiologia* 364:65–74.
- Hargrave, B. T. 1972. Aerobic decomposition of sediment and detritus as a function of particle surface area and organic content. *Limnology and Oceanography* 17:583–596.
- Hilsenhoff, W. L. 1966. The biology of *Chironomus plumosus* (Diptera: Chironomidae) in Lake Winnebago, Wisconsin. *Annals of the Entomological Society of America* 59:465–473.
- Hölker, F., M. J. Vanni, J. J. Kuiper, C. Meile, H.-P. Grossart, P. Stief, R. Adrian, A. Lorke, O. Dellwig, A. Brand, M. Hupfer, W. M. Mooij, G. Nützmann, and J. Lewandowski. 2015. Tubedwelling invertebrates: tiny ecosystem engineers have large effects in lake ecosystems. *Ecological Monographs* 85:333–351.
- Jørgensen, B. B., and N. P. Revsbech. 1985. Diffusive boundary layers and the oxygen uptake of sediments and detritus. *Limnology and Oceanography* 30:111–122.
- Kristensen, E., G. Penha-Lopes, M. Delefosse, T. Valdemarsen, C. O. Quintana, and G. T. Banta. 2012. What is bioturbation? The need for a precise definition for fauna in aquatic sciences. *Marine Ecology Progress Series* 446:285–302.
- Lewandowski, J., and M. Hupfer. 2005. Effect of macrozoobenthos on two-dimensional small-scale heterogeneity of pore water phosphorus concentrations in lake sediments: a laboratory study. *Limnology and Oceanography* 50:1106–1118.

- Lorke, A., D. F. McGinnis, A. Maeck, and H. Fischer. 2012. Effect of ship locking on sediment oxygen uptake in impounded rivers. *Water Resources Research* 48:1–7.
- Lorke, A., B. Müller, M. Maerki, and A. Wüest. 2003. Breathing sediments: the control of diffusive transport across the sediment–water interface by periodic boundary-layer turbulence. *Limnology and Oceanography* 48:2077–2085.
- Lorke, A., and F. Peeters. 2006. Toward a unified scaling relation for interfacial fluxes. *Journal of Physical Oceanography* 36:955–961.
- Matisoff, G., and X. Wang. 1998. Solute transport in sediments by freshwater infaunal bioirrigators. *Limnology and Oceanography* 43:1487–1499.
- Mermillod-Blondin, F., R. Rosenberg, F. François-Carcaillet, K. Norling, and L. Mauclair. 2004. Influence of bioturbation by three benthic infaunal species on microbial communities and biogeochemical processes in marine sediment. *Aquatic Microbial Ecology* 36:271–284.
- Morad, M. R., A. Khalili, A. Roskosch, and J. Lewandowski. 2010. Quantification of pumping rate of *Chironomus plumosus* larvae in natural burrows. *Aquatic Ecology* 44:143–153.
- Munksby, N., M. Benthien, and R. N. Glud. 2002. Flow-induced flushing of relict tube structures in the central Skagerrak (Norway). *Marine Biology* 141:939–945.
- Murniati, E., S. Geissler, and A. Lorke. 2015. Short-term and seasonal variability of oxygen fluxes at the sediment–water interface in a riverine lake. *Aquatic Sciences* 77:183–196.
- Murniati, E., D. Gross, H. Herlina, K. Hancke, R. N. Glud, and A. Lorke. 2016. Oxygen imaging at the sediment-water interface using lifetime-based laser induced fluorescence (τ LIF) of nano-sized particles. *Limnology and Oceanography: Methods* 17:506–517.
- Papkovsky, D. B., and R. I. Dmitriev. 2013. Biological detection by optical oxygen sensing. *Chemical Society Reviews* 42:8700–8732.
- Pelegri, S. P., and T. H. Blackburn. 1996. Nitrogen cycling in lake sediments bioturbated by *Chironomus plumosus* larvae, under different degrees of oxygenation. *Hydrobiologia* 325:231–238.
- Pinder, L. C. V. 1986. Biology of freshwater Chironomidae. *Annual Review of Entomology* 31:1–23.
- Polerecky, L., N. Volkenborn, and P. Stief. 2006. High temporal resolution oxygen imaging in bioirrigated sediments. *Environmental Science and Technology* 40:5763–5769.
- Roskosch, A., N. Hette, M. Hupfer, and J. Lewandowski. 2012. Alteration of *Chironomus plumosus* ventilation activity and bioirrigation-mediated benthic fluxes by changes in temperature, oxygen concentration, and seasonal variations. *Freshwater Science* 31:269–281.
- Roskosch, A., M. Hupfer, G. Nützmann, and J. Lewandowski. 2011. Measurement techniques for quantification of pumping activity of invertebrates in small burrows. *Fundamental and Applied Limnology* 178:89–110.
- Roskosch, A., M. R. Morad, A. Khalili, and J. Lewandowski. 2010. Bioirrigation by *Chironomus plumosus*: advective flow investigated by particle image velocimetry. *Journal of the North American Benthological Society* 29:789–802.
- Sacksteder, L., J. N. Demas, and B. A. DeGraff. 1993. Design of oxygen sensors based on quenching of luminescent metal complexes: effect of ligand size on heterogeneity. *Analytical Chemistry* 65:3480–3483.
- Soster, F. M., G. Matisoff, D. W. Schloesser, and W. J. Edwards. 2015. Potential impact of *Chironomus plumosus* larvae on hypolimnetic oxygen in the central basin of Lake Erie. *Journal of Great Lakes Research* 41:348–357.
- Stief, P., L. Nazarova, and D. de Beer. 2005. Chimney construction by *Chironomus riparius* larvae in response to hypoxia: microbial implications for freshwater sediments. *Journal of the North American Benthological Society* 24:858–871.
- Volkenborn, N., L. Polerecky, D. S. Wetthey, and S. A. Woodin. 2010. Oscillatory porewater bioadvection in marine sediments induced by hydraulic activities of *Arenicola marina*. *Limnology and Oceanography* 55:1231–1247.
- Walshe, B. M. 1947. Feeding mechanisms of *Chironomus* larvae. *Nature* 160:474.
- Walshe, B. M. 1950. The function of haemoglobin in *Chironomus plumosus* under natural conditions. *Journal of Experimental Biology* 27:73–95.
- Woodin, S. A., D. S. Wetthey, and N. Volkenborn. 2010. Infaunal hydraulic ecosystem engineers: cast of characters and impacts. *Integrative and Comparative Biology* 50:176–187.
- Yeh, T.-S., C.-S. Chu, and Y.-L. Lo. 2006. Highly sensitive optical fiber oxygen sensor using Pt(II) complex embedded in sol-gel matrices. *Sensors and Actuators B: Chemical* 119:701–707.